A Photoacoustic-Based Measurement System for Dual Detection of NO_2 and CO_2 in Combustion Exhaust Gases

Enza Panzardi, *Member, IEEE*, Klaus Stefan Drese, Marco Mugnaini, Lorenzo Parri, Valerio Vignoli, *Member, IEEE*, and Ada Fort, *Member, IEEE*

***Abstract*— In this article, a low-cost, low-complexity photoacoustic (PA) sensing system for the simultaneous detection of CO_2 and NO_2 in exhaust gas is presented. The proposed system is designed as part of a continuous emissions monitoring system (CEMS) for gas turbine emissions. The system exploits the amplification of the PA signal provided by an acoustic ring resonator, which is characterized by a simple and robust structure and is suitable for in-field measurements. The dual gas detection is obtained by exploiting two measurement principles; the first one, dedicated to the detection of NO_2, which is present in the target mixture in the ppm range, is the classical PA effect. In fact, the optical source is a light-emitting diode (LED) with a center wavelength of 405 nm matched on an adsorption peak of NO_2. This allows for deriving the NO_2 concentration measurement directly from the amplitude of the PA signal. The other mechanism is used to measure the concentration of one of the major components of the exhaust gas, with a concentration in the range of some percentage. The quantity of CO_2 is sensed, exploiting its effect on the sound speed, and consequently on the resonance frequency of the resonator. To measure the CO_2 concentration, the system automatically tracks the acoustic resonance shift. The detection of the two gases is realized simultaneously by a unique sensor with real-time measurements. A laboratory characterization of the proposed systems showed its feasibility. Experimental results show the possibility to detect NO_2 with a resolution lower than 1 ppm, whereas CO_2 resolution is about 0.2%.**

***Index Terms*— CO_2 sensor, combustion emission monitoring, gas measurement system, NO_2 sensor, photoacoustic (PA) gas sensors, resonant sensor.**

I. Introduction

THE monitoring and analysis of the composition of exhaust gases from gas turbines, which are widely used in power generation and aircraft propulsion, is a widely used tool not only for controlling polluting emissions to ensure compliance with official regulations in terms of air quality but also for the optimization of the plant operations [1], [2], [3]. In fact, gas emission monitoring has a prominent role in turbomachinery condition monitoring (i.e., gas turbines and combined cycle plants) since it provides direct information concerning the health and the performance of the combustion plant components (the burner, the compressor, and the fueling system), as well as the fuel quality [4], [5], [6]. Typically, the concentration of gases in the exhaust flow of turbomachinery can vary depending on various factors such as the type of turbine, the fuel composition, the operating conditions, and the specific application [5]. If we consider as a reference the typical exhaust emissions from a stationary gas turbine of one of the world's most popular industries used for marine and industrial applications (i.e., the General Electric Industry), the emission composition can be summarized, as in Table I [7].

TABLE I
GAS TURBINE EXHAUST EMISSIONS OBTAINED BY BURNING CONVENTIONAL FUELS

Gas species	Typical concentration % Volume	Gas species	Typical concentration ppm Volume
Nitrogen (N_2)	66 – 72	Nitric Oxide (NO)	20 - 220
Oxygen (O_2)	12 – 18	Nitrogen Dioxide (NO_2)	2 - 20
Carbon Dioxide (CO_2)	1 - 5	Carbon Monoxide (CO)	5 - 330
Water Vapor (H_2O)	2- 10	Sulphur Dioxide (SO_2)	trace - 100
		Sulphur Trioxide (SO_3)	trace - 4
		Unburned Hydrocarbons (UHC)	5 - 300
		Particulate Matter (PM)	trace - 25

Table I provides evidence to distinguish between two categories of components: those present in percentage concentrations and those present in parts per million (ppm). The latter category mainly consists of pollutant components aside from CO and NO_x, which are unwanted byproducts of the combustion of fossil fuels [8]. The theoretical concentration of major components, such as CO_2 or O_2, can typically be calculated for a combustion process by knowing the operating conditions of the plant and the quality of the fuel [9].

Manuscript received 25 July 2023; revised 7 October 2023; accepted 14 October 2023. Date of publication 30 October 2023; date of current version 10 November 2023. This work was supported by the European Union—FSE REACT-EU, PON Ricerca e Innovazione 2014–2020. The Associate Editor coordinating the review process was Dr. Nuria Novas. *(Corresponding author: Enza Panzardi.)*

Enza Panzardi, Marco Mugnaini, Lorenzo Parri, Valerio Vignoli, and Ada Fort are with the Department of Information Engineering and Science, University of Siena, 53100 Siena, Italy (e-mail: enza.panzardi@unisi.it; marco.mugnaini@unisi.it; lorenzo.parri@unisi.it; valerio.vignoli@unisi.it; ada.fort@unisi.it).

Klaus Stefan Drese is with the Institute of Sensor and Actuator Technology, Coburg University of Applied Sciences and Arts, 96450 Coburg, Germany (e-mail: klaus.drese@hs-coburg.de).

Digital Object Identifier 10.1109/TIM.2023.3328691

It is, however, crucial to note that under malfunctioning plant conditions or with low-quality fuel, the measured component concentrations may deviate from expected values [8], [9]. In contrast, pollutant component concentrations can never be predetermined, making accurate measurement essential for assessing combustion quality and complying with air pollutant limits [10]. These measurements require careful and often costly procedures.

Measuring both percentage and ppm (and even ppb) values using a single technique presents significant challenges due to the different concentration scales involved. These challenges stem from limitations in measurement principles and instrument capabilities.

Several measurement techniques can offer a wide measurement range of gas concentration by employing appropriate calibration and adjustment procedures or using highly accurate and advanced instrumentation to cover both percentage and ppm values. Among these, gas chromatography (GC) with flame ionization detection (FID) allows for the measurement of a broad concentration range achieved by adjusting the sample injection volume or using different detector settings [11], [12], [13]. Similarly, infrared (IR) spectroscopy [14] can be employed with different pathlength cells to adjust sensitivity: shorter pathlength cells can be used for higher concentrations (percentage), while longer pathlength can be used to sense lower concentrations (ppm) [15], [16], [17]; however, most of these are expensive laboratory techniques.

Photoacoustic (PA) detection has gained considerable attention in emissions monitoring due to its high sensitivity to trace gases, making it a valuable and versatile solution for gas measurement and analysis, above all in scenarios involving low concentrations [18], [19]. The PA gas detection exploits the PA effect, i.e., the generation of pressure waves due to the selective adsorption of optical power, which locally heats the gas present in the optical path. The generation of the acoustic wave requires dynamic heating, i.e., a time variable power transferred to the gas achieved by dynamically driving the optical source. The acoustic signal amplitude is related to the concentration of the absorbing gas and is sensed by means of microphones or ultrasonic transducers. A particularly promising solution exploiting PA detection is the one that enhances the sensitivity of acoustic detection by means of acoustic resonators [20], [21]. In resonant PA measurement systems, the measurement cell, where the gas interacts with the light, is an acoustic resonator, and the light is intensity-modulated with a frequency tuned to its resonance, thereby exploiting the amplification of the resonant structure. These systems can be coupled to tuned narrowband front-end electronics, and this allows for further increasing the signal-to-noise ratio (SNR). The acoustic resonance frequency is determined by the geometry of the measurement chamber and by the sound speed [22], [23]. Having a narrowband acoustic readout system has the advantage of improving the sensitivity of the system and reducing external interference but poses some issues. In fact, the measurement systems must always operate tuned to the acoustic resonance; otherwise, the amplitude of the PA signal will change, not due to target gas adsorption but due to the frequency response of the system [22]. If the analyzed gas has always the same composition but for gases with concentrations in the ppm range, as in the case of environmental monitoring where air is the carrier gas and the additional compounds, i.e., the pollutants are in the ppm ranges, the sound speed will experience variations in the order of ppm too, and resonant frequency can be assumed as independent of the mixture composition. In these cases, the optical source driving system can operate at a fixed frequency, with no need to track the acoustic resonance. On the other hand, for those applications in which the gas composition varies in higher concentrations (i.e., in the percent scale), the sound speeds can appreciably vary; therefore, the variation of the PA signal intensity due to the acoustic resonance shift effect cannot be neglected [24].

In this work, we show the feasibility of a measurement technique dedicated to the double detection of CO_2 and NO_2 in the exhaust gases of industrial plants, exploiting the resonant PA measurement principle and the tracking of the gas measurement cell acoustic resonance.

Our system is designed as part of a continuous emissions monitoring system (CEMS) for gas turbine emissions. CEMS are comprehensive solutions that combine various gas analyzers, sample conditioning systems, data acquisition equipment, and software for continuous emissions monitoring. These instruments (few available on the market) primarily rely on electrochemical sensors.

The significant advantage of our proposed technique lies in its reliance solely on physical interactions with target gases without involving chemical reactions. Consequently, no components of the sensing system undergo transformation or consumption. This feature greatly extends the lifespan of the sensing systems, eliminates the need for periodic calibrations or sensor replacements, and improves the overall performance in gas turbine combustion monitoring and control applications.

PA sensing, moreover, offers unique advantages in terms of noncontact, real-time monitoring of specific gas species, especially when used with resonance-enhanced setups. In contrast, as far as alternative methods for analyzing combustion exhaust gases are concerned, IR spectroscopy is versatile but often complex and costly. GC is accurate but unsuitable for real-time monitoring; tunable diode laser absorption spectroscopy (TDLAS) is highly sensitive but can be complex and expensive. FID focuses on hydrocarbons, and mass spectrometry (MS) provides unmatched sensitivity and selectivity, albeit at higher costs and complexity.

As shown in Table I, the NO_2 concentration in the exhaust flow ranges between 2 and 20 ppm, whereas the CO_2 concentration is in the interval 1%–5%. In the application of interest, the variation of the concentration of the major components of the exhaust gas (such as CO_2) appreciably changes the speed of sound; so, in this article, we propose a PA detection system in which the light modulation frequency tracks the resonance frequency of the acoustic resonator. This frequency is measured to determine the concentration of the major components of the exhaust gas, and thus, to derive the one of CO_2, whereas the intensity of the PA signal at the tuned frequency is used to measure the concentration of NO_2. Although the measurement of the speed of sound remains a widely employed method in gas sensing applications, its

combination with the PA effect for gas mixture analysis is novel [25], [26].

Recently, Wang et al. [27] demonstrated the feasibility to use a combined PA and resonance frequency tracking (RFT) technique for the detection of methane gas (CH_4), in a wide concentration range: the measurement of concentrations up to 30% exploits PA detection, above this value the system switches to the RFT measurement. They used a tunable distributed feedback diode laser (DFB-LD) as a light excitation source for the PA detection.

In summary, in this study, we introduce a novel approach that combines the PA and RFT measurement techniques to concurrently quantify two distinct gas species: NO_2 and CO_2. Our focus is on the application of exhaust emission monitoring in gas turbines.

The proposed system relies on the measurement of the magnitude of a PA signal to measure parts per million (ppm) variations in the concentration of NO_2 within the monitored gas flow. To achieve this, we employ an ultraviolet light-emitting diode (UV-LED) emitting light in a spectrum that encompasses an absorption peak specific to NO_2 but avoids the absorption peaks of other exhaust gas components. Additionally, we monitor the concentration of CO_2, which falls within the range of a few percent, by continuously tracking the resonant frequency of the PA cell.

II. Theoretical Background

This section will provide a detailed description of the measurement principles for simultaneously measuring NO_2 and CO_2 concentrations in exhaust gases. Section II-A will cover the PA sensing of NO_2 enhanced by the use of an acoustic resonant PA cell, while Section II-B will illustrate the detection of CO_2. CO_2 does not selectively absorb light at the operating wavelength but causes a significant variation in sound speed. Its detection is based on the dependence of the eigenmode frequency of an acoustic resonator on the sound speed.

A. PA Sensing of NO_2

The origins and operations of PA and PA spectroscopy (PAS) gas sensing systems are rooted in the PA effect, first discovered by Alexander Graham Bell in 1880 [28]. This effect pertains to the ability to absorb energy from photons and convert it into acoustic energy [29].

In the context of gas sensing, a portion of gas enclosed in a specific volume is exposed to an intensity-modulated light source. In the following, a sinewave modulation is considered with frequency f_m ($f_m = \omega_m/2\pi$, ω_m is the intensity modulation angular frequency). The wavelength of the light source, denoted as λ, is chosen to match one of the peaks in the absorption spectrum of the gas being monitored. Consequently, the absorbed light excites the target gas molecules, causing local and time-varying thermal expansion. This, in turn, generates an acoustic wave with a frequency given by the modulation of the light source [29], which propagates through the gas and can be detected using an acoustic transducer, such as a sensitive microphone.

The resulting acoustic wave $p(\boldsymbol{r}, \omega)$, is typically weak in intensity, therefore, a good option is boosting its amplitude by resonant amplification using a resonant-based setup [20], [30].

In more detail, in a resonant PA cell, the acoustic wave can be described in the angular frequency domain through an eigenmode expansion as a function of the position, $\boldsymbol{r}$, with the following equation [31], [32]:

$$p(\boldsymbol{r}, \omega) = (\gamma - 1)\alpha I_0 \left(\frac{L_{\text{cell}}}{j\omega V_{\text{cell}}} + \sum_n \frac{L_{\text{cell}}}{V_{\text{cell}}} \frac{j\omega F_n s_n(\boldsymbol{r})}{\omega_n^2 - \omega^2 + j\frac{\omega\omega_n}{Q_n}} \right) \tag{1}$$

where α represents the gas absorption coefficient at a given λ. For low concentration of the target gas, α is related to the number density of the gas molecules, N, and to the absorption cross-section $\sigma(\lambda)$, through $\alpha = N\sigma(\lambda)$; moreover, γ is the specific heat ratio of the gas, I_0 is the incident power generated by the optical source, Q_n is the quality factor of the nth eigenmode with angular frequency ω_n, F_n is the mode shape factor, whereas $s_n(r)$ describes its spatial distribution. L_{cell} and V_{cell} are, respectively, the length and the volume of the PA cell [31]. Note that the modal frequencies (or resonance frequencies) depend on the PA cell geometry and are all proportional to the speed of sound, such that $\omega_n \propto c$.

To ensure sufficient sensitivity of the system, the wavelength of the optical source is carefully chosen to grant a sufficiently high absorption cross-section, $\sigma(\lambda)$, for the target gas, specifically within one of the gas absorption peaks. It can be observed that the PA signal is amplified effectively by modulating the light source to match one of the acoustic resonances of the gas enclosure (i.e., the PA cell). This is achieved by selecting the frequency of the light modulation signal, f_m, to coincide with one of the eigenmode ($n = r$) frequencies such that $f_m = f_r = (\omega_r/2\pi)$ and the amplitude of the selected resonance mode is amplified by a factor proportional to the quality factor Q_r while the amplitude of the other resonances is limited by the terms $\omega_n^2 - \omega_r^2$, with $r \neq n$, at the denominator of (1).

Exciting the PA cell through the tuning of an eigenmode, results in a standing wave pattern characterized by nodes (zero acoustic pressure) and antinodes (maximum acoustic pressure). The wave amplitude, P, should be measured at an antinode of the PA cell.

In this configuration, the cell acts as a natural amplification stage, significantly improving the SNR of the system. In fact, the measured signal amplitude, P, can be well approximated by

$$P = \alpha I_0 F_s \frac{L_{\text{cell}}}{V_{\text{cell}}} \frac{Q_r}{\omega_r} (\gamma - 1) \tag{2}$$

where F_s is obtained by spatially integrating the term in (1) that describes the spatial distribution of the wave over the microphone receiving lobe [31].

Equation (2) clarifies how the acoustical resonance of the cell amplifies the PA signal. In fact, the acoustic pressure magnitude, besides depending linearly on the optical excitation intensity on the ratio between the length and volume of the PA cell, varies with the Q factor of the eigenmode.

Conversely, P is inversely related to the operating frequency (the lowest modes are preferable).

Finally, as per (1), the PA signal amplitude, P, is directly proportional to the gas concentration (expressed in terms of density of gas molecules, N) through the absorption coefficient; therefore, the PA signal amplitude for small concentration, varies linearly with the gas concentration, enabling its measurement.

As the gas concentration increases, the absorption capacity of gas molecules, however, becomes nonlinear until it reaches the maximum limit, which causes the saturation of the PA signal amplitude [33].

B. Measurement of CO_2 Concentration Through RFT

As discussed in the introduction and clarified with (1) and (2), the eigenfrequencies of the PA cell depend on the speed of sound c ($f_r \propto c$) [32].

This latter depends on the chemical composition, temperature, and pressure of the gas. For a single ideal gas, the sound speed can be found as follows [26], [34]:

$$c = \sqrt{\frac{\gamma RT}{M_g}} \tag{3}$$

where R is the universal gas constant ($8.314\ \mathrm{J \cdot mol^{-1} \cdot K^{-1}}$), T is the temperature of the gas (in Kelvin), and M_g is the gas molar mass.

Assuming to operate at constant temperature and pressure (a reasonable assumption for this work) and in case of a mixture of K gases, both M_g and γ will be derived from the characteristics of the individual gas components, as follows:

$$\gamma = \frac{\sum_{i=1}^{K} C_{Y_i} c_{p_{Y_i}}}{\sum_{i=1}^{K} C_{Y_i} c_{v_{Y_i}}} \quad M_g = \sum_{i=1}^{K} C_{Y_i} M_{Y_i}$$
$$i = 1, 2, \ldots, K \text{ gas component} \tag{4}$$

where $c_{p_{Y_i}}$ and $c_{v_{Y_i}}$ are the specific heats at constant pressure and volume, respectively, of the Y_i species, M_{Y_i} is its molar mass whereas C_{Y_i} is its volume concentration.

From (3) and (4), it can be deduced that when there is a significant variation of the composition of the analyzed gas, this will result in a significant change of the speed of sound, and thus, in a measurable shift of the resonance frequency of PA cell ($\Delta f_r \propto \Delta c$, $\Delta c^2 \approx ((RT(\gamma \Delta M_g - \Delta \gamma M_g))/M_g^2)$). In particular, with reference to the monitoring of the methane (CH_4) combustion exhaust flux, by ignoring the components that are present in ppm values, the stoichiometric combustion reaction is given by [9]

$$CH_4 + 2O_2 \rightarrow CO_2 + 2H_2O. \tag{5}$$

In the present application, given a certain fuel/air ratio, the following volume concentration for the major components is found at the input of the combustion system:

$$C_{N_2} = (1-x)0.79; \quad C_{O_2} = (1-x)0.21; \quad C_{CH_4} = x \tag{6}$$

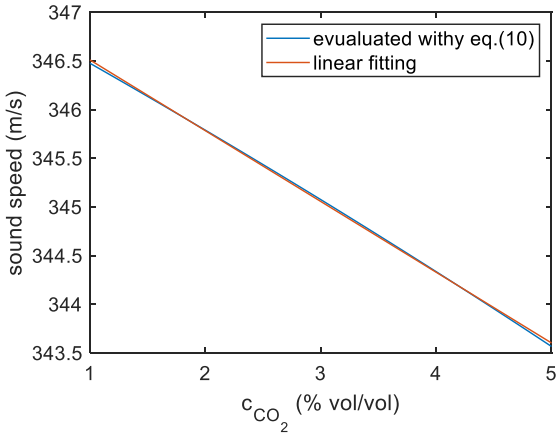

Fig. 1. Speed of sound in the dried and cooled gas exhaust as a function of the CO_2 evaluated according to (10) at 25 °C.

where x is the fuel concentration. At the exhaust of the combustor, the expected concentration of the major components for a perfect combustion will be

$$C'_{N_2} = (1-x)0.79; \quad C'_{O_2} = (1-x)0.21 - 2x; \quad C'_{C0_2} = x;$$
$$C'_{H_2O} = 2; \quad xC'_{CH_4} = 0. \tag{7}$$

In a real combustion, a deviation (δ) from this ideal situation can be expected, and the major component concentrations will be

$$C'_{N_2} = (1-x)0.79; \quad C'_{O_2} = (1-x)0.21 - 2(x-\delta);$$
$$C'_{C0_2} = x - \delta; \quad C'_{H_2O} = 2(x-\delta); \quad C'_{CH4} = \delta. \tag{8}$$

Finally, considering that the water is almost removed by the gas sampling system (brought by the chiller in the 10^{-3} concentration range) before reaching the measurement device, the gas mixture in the PA detector will have the following composition:

$$C''_{N_2} = \frac{(1-x)}{1-2(x-\delta)}0.79; \quad C''_{C0_2} = \frac{x-\delta}{1-2(x-\delta)};$$
$$C''_{O_2} = \frac{(1-x)}{1-2(x-\delta)}0.21 - \frac{2(x-\delta)}{1-2(x-\delta)} \tag{9}$$

therefore, the speed of sound in the measurement chamber can be expressed as in (10), shown at the bottom of the page.

In the considered application, the CO_2 concentration ranges from 1% to 5%; therefore, the expected variation of the sound speed is considerable, and in the ranges of some percentages too, as shown in Fig. 1.

The relationship between sound speed and CO_2 concentration is approximately linear, with a slope of about -0.72 (m/s)/%CO_2 and a maximum nonlinearity error (NLE) of 0.64% (of the span).

This variation of the sound speed in resonant-based PA gas sensing setups that operate with a fixed frequency optical source modulation, not granting that f_m is equal to the resonance frequency f_r in any working conditions, will have

$$c^2 = \frac{RT\left(C''_{N_2} c_{p_{N_2}} + C''_{O_2} c_{p_{O_2}} + C''_{CO_2} c_{p_{CO_2}}\right)}{\left(C''_{N_2} c_{v_{N_2}} + C''_{O_2} c_{v_{O_2}} + C''_{O_2} c_{v_{CO_2}}\right)\left(C''_{N_2} M_{N_2} + C''_{O_2} M_{O_2} + C''_{CO_2} M_{CO_2}\right)} \tag{10}$$

an impact on the accuracy of the measurements because the resonance of the PA cell changes by changing the CO_2 concentration. Specifically, in this scenario, the amplitude of the PA signal amplitude is influenced by the displacement of the frequency response peak of the PA cell, i.e., by the difference between f_m and f_r.

A PA resonant system used in the context of interest, must therefore, operate by adapting f_m to the PA cell eigenmode frequency in any measurement conditions, i.e., with any concentration of CO_2. This means that the system must embed a RFT technique.

The tracked resonance can then be exploited for a direct measurement of the CO_2 concentration since $f_r \propto c$.

It should be noted that although the percentage concentration of a gas in a mixture greatly affects the resonant frequency of the acoustic cell, the intensity of the PA signal generated by the gas–light interaction, on the other hand, depends just on the light absorption capability of the gas according to its absorption spectrum (thus, on the wavelength of the selected optical source).

III. Measurement System and Processing Technique

A. Measurement Setup

The laboratory measurement setup used to illustrate the feasibility of the proposed technique is depicted in Fig. 2. Specifically, Fig. 2(a) presents its block diagram, while Fig. 2(b) provides a photograph of the overall measurement setup and details of the PA cell.

The developed measurement technique is based on exciting a PA signal in the acoustic resonator [PA cell in Fig. 2(a)], using an optical source [LED in Fig. 2(a)] that among the different compounds present in the exhaust gas, is adsorbed by NO_2 only. The ring resonator shown in Fig. 2(b) [31] is the used PA cell. With this geometry, the first eigenmode is characterized by two nodes situated at the endpoints of a diameter and two antinodes positioned at the endpoints of a diameter perpendicular to the first [31]. The LED position determines the illuminated region, and thus, one antinode position and the microphone is placed at the other antinode, where the acoustic pressure is maximized, thereby optimizing the SNR of the system. On the other hand, the gas flow openings are strategically placed at the pressure nodes to minimize acoustic losses.

The LED is driven by an ad hoc designed driver hosted in the front electronic board, which amplifies the signal generated by an arbitrary waveform generator [AWG in Fig. 2(a)]. The same board also contains the conditioning electronics for the PA signal, sensed by a microphone, which is then acquired through an A/D board and processed by a PC. The PC also manages the whole experiment through a virtual instrument (VI) in a LabView environment.

In detail, the used optical source is a UV-LED manufactured by Stanley Electric (NDU1104ESE) with a peak wavelength $\lambda_{peak} = 405$ nm and a maximum expected wavelength shift of 15 nm. The choice of this LED was based on previous findings by Fort et al. [31], which presented a resonant-based PA

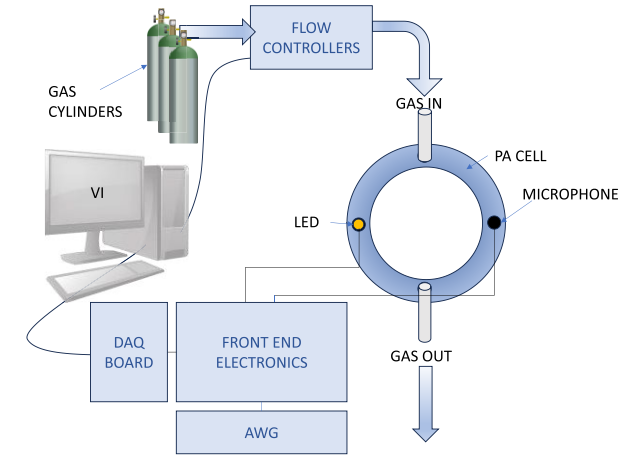

(a)

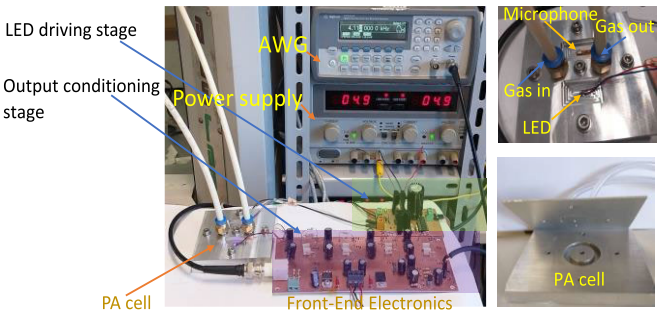

(b)

Fig. 2. Measurement system setup. (a) Schematic representation. (b) Photographs of the overall measurement setup.

sensor for NO_2 detection in low concentration. The LED was selected to attain light absorption by the NO_2 gas, which has a prominent absorption peak at this wavelength and a spectral amplitude around λ_{peak} adequate to cover any peak wavelength change during real operation [21], [35]. Simultaneously, this choice avoids absorption interference from CO_2, oxygen, and N_2. By doing so, it prevents any absorption interference on the generated PA signal. Additionally, the LED is a cost-effective solution that can be easily incorporated into a low-power system, and it serves as an ideal solution for resonance tracking since the illuminating beam can be easily manipulated by controlling the driving current. The exciting current in this work is set by means of an AWG by Agilent Technologies (AG33220), which is appropriately configured to produce a sinusoidal current with a maximum peak-to-peak amplitude I_{outpp} of 200 mA at the desired modulation frequency f_m.

The PA cell [see Fig. 2(a) and (b)] consists of a ring-shaped structure made of polished aluminum; it has a volume of 3.3 cm^3 and a Q-factor of approximately 28 [31]. The design and dimensions of the cell were optimized to enhance the pressure/acoustic sensitivity of the system while still ensuring high performance in terms of response time and robustness against influence quantities, as discussed in detail by Fort et al. [31]. The resonance frequency of the first eigenmode of the cell was evaluated through finite element simulations both in air and nitrogen and experimentally validated when operating in pure N_2, yielding a value of $f_r = 4112$ Hz.

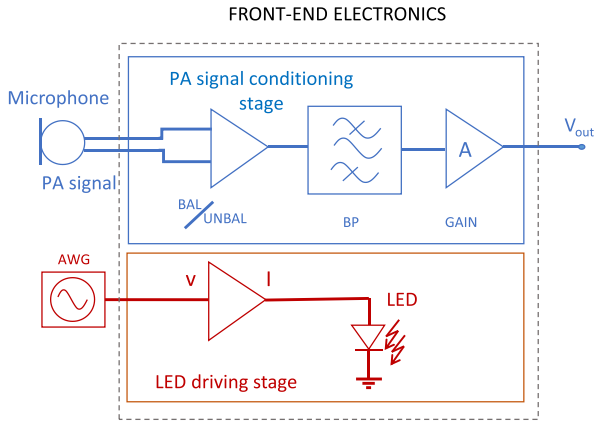

Fig. 3. Front-end board schematic.

It should be noted that the molar mass of air and N_2 is approximately the same: the molar mass of air is approximately 28.97 g/mol, while the molar mass of N_2 is approximately 28.02 g/mol. As a result, the speed of sound, and thus, the frequency f_r, in these two media does not deviate significantly.

The top side of the cell embeds a total of four holes; two are dedicated to the inlet and outlet of the gas, while the remaining are needed to house the light source (LED) and the microphone employed for the PA signal detection.

The microphone used is a low-noise MEMS microphone manufactured by STMicroelectronics (MP23AB02B).

The front-end electronics (whose schematic is reported in Fig. 3) is responsible for properly adapting the driving current for the LED and for conditioning the PA signal detected by the microphone for the acquisition and processing tasks. In particular, the detected PA signal passes through a preamplification stage that converts the unbalanced output of the microphone to a balanced one, then properly amplified, and the band passed in a specific range of frequencies around f_r. The electronics must be designed so as to avoid distortion for any possible shift due to the gas composition change inside the cell; at the same time, it has to be as narrow a band as possible to limit external acoustic interferences.

In this work, the system bandwidth (−3 dB) was set to 500 Hz, centered on the cell resonant frequency f_r, evaluated in N_2. The PA signal is acquired by a 16-bit data acquisition board (DAQ, NI PCI601) with a maximum sampling rate of 200 kS/s. The desired gas flow injected into the PA cell during tests is achieved using an accurate flowmeter system (Bronkhorst F-201C, 100 mL full-scale accuracy ±0.5% reading plus ±0.1% full-scale). This system is digitally controlled by the user, allowing for adjustments of the gas concentration, mixture composition, and total flow. In this study, the total flow is maintained constant at 100 mL/min throughout the measurements. The different gases are provided by a specialized company (SOL, S.p.a) in certified gas cylinders of 50 L. All the mixtures used in the test are obtained by combining different flows of three reference mixtures, in detail exploiting certified cylinders of CO_2 diluted in N_2 at the concentration of 20% (2% tolerance), pure N_2, and 50 ppm NO_2 (10% tolerance) in N_2.

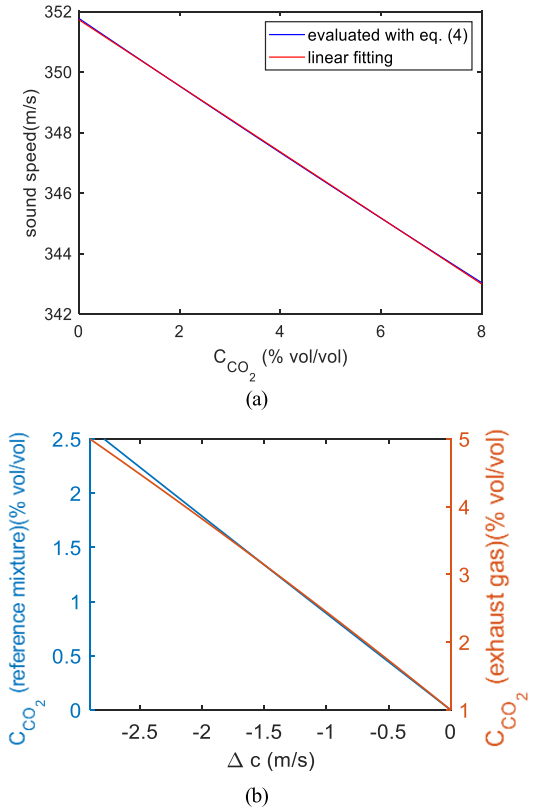

Fig. 4. (a) Sound speed as a function of the CO_2 concentration in the reference mixture used for laboratory experiments at 25 °C evaluated according to (4). (b) CO_2 concentration variation versus variation of the sound speed at 25 °C left axis: for the reference mixture, right axis: according to (10).

B. Measurement Protocol

The feasibility and the performance of the proposed measurement technique were investigated by means of laboratory experiments, using mixtures of N_2, CO_2, and NO_2 to emulate conditions like those expected during operations but in controlled and reference conditions. The PA effect was, therefore, exploited to measure the variation of the NO_2 in the flow under test (FUT) in the range between 1 and 50 ppm, whereas the tracking of the cell resonance frequency is used to discriminate concentrations of CO_2 varying up to 8%.

In Fig. 4(a), the variation of the sound speed expected when varying the concentration of CO_2 in the gas mixtures used for laboratory tests is shown. It can be seen that the variation is almost linear with CO_2 concentration, with a NLE of about 0.47% of the span: the slope of the linear fitting is -1 (m/s)/%CO_2. Fig. 4(b) shows how the sound speed varies in the two situations as a function of CO_2, showing that the laboratory tests will reproduce situations very similar to those related to the application of interest.

C. Automated Measurement System

As already said, the experiments are managed by the PC running various VIs developed with the National Instruments LabVIEW design software. A main VI (see the front panel in Fig. 5) permits performing the fully automatic measurements, and in detail, it allows setting the AWG used for system excitation, setting the flow meters to gather data in different gas

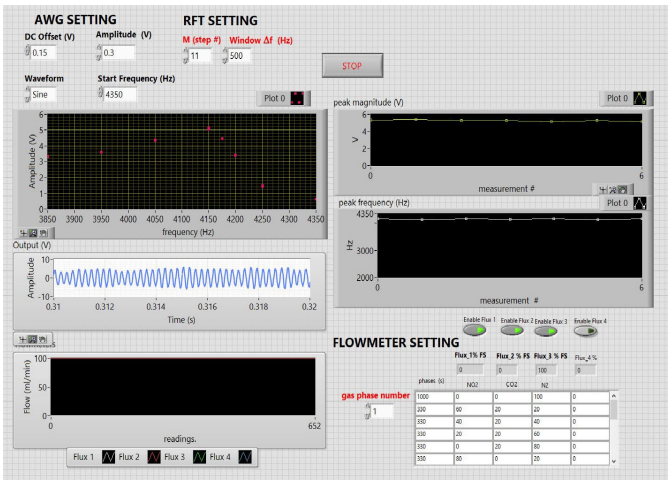

Fig. 5. Front panel of the VI used to perform automatic measurements.

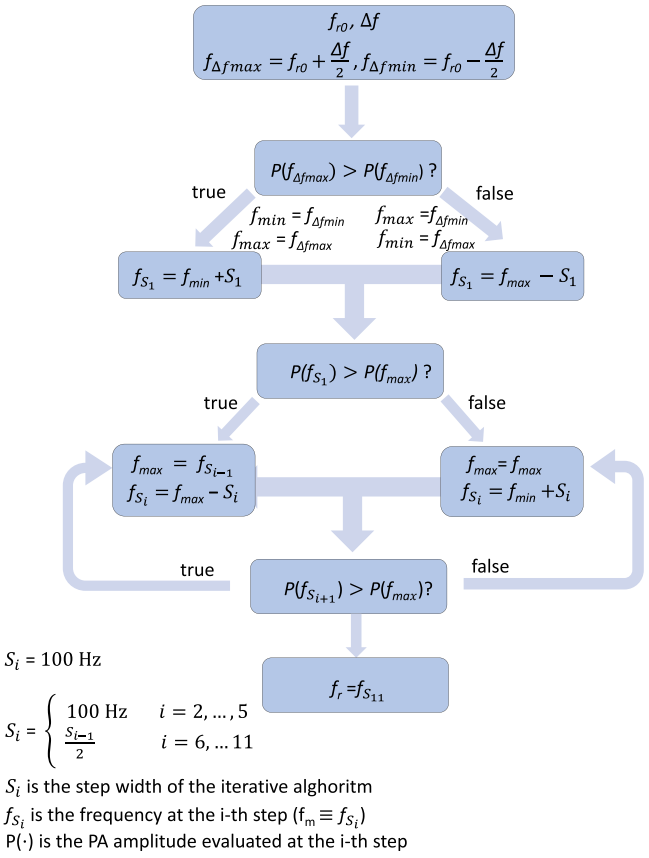

Fig. 6. Flow diagram of the iterative frequency tracking algorithm.

compositions, handling the acquisition task, and the processing of the PA signal, and finally to save data.

In particular, the VI allows for setting the LED excitation current amplitude and runs the RFT algorithm, thereby adjusting the LED excitation frequency f_m, tracking the resonance of the PA cell within a selected frequency window, Δf. Additionally, the system provides the option to choose Δf and the number of steps, M, for executing the RFT algorithm. The algorithm employs a closed-loop control system encompassing the PC. It iteratively adjusts the excitation frequency within the predefined range, comparing the amplitudes of the acquired PA signals to find the frequency that yields the highest signal amplitude.

This iterative process continues for a specified number of steps (M), with each step involving signal acquisition and analysis, taking an adjustable time for signal analysis, T_{meas}, (typically several tens of milliseconds). This real-time operation ensures that the RFT procedure adapts the working frequency of the PA cell in MT_{meas} seconds.

In detail, the executed RFT algorithm (whose flow diagram is shown in Fig. 6) is designed to change the modulation frequency, searching for the maximum amplitude of the PA signal in M steps. During each step S_i ($i = 1, \ldots, M$), a frequency f_{Si} is used to excite the optical source, a fixed time window of the PA signal is acquired (with a selectable duration of $T_w < T_{\text{meas}}$), and its amplitude, $P(f_{Si})$, is evaluated by means of an accurate single-tone frequency digital estimation method. The length of the time windows, $T_{w,}$ is set to 200 ms in this work. The algorithm spans the interval Δf, moving toward the frequency at which the response exhibits the highest amplitude. This is achieved by comparing the PA signal amplitude evaluated at each step with the value estimated in the previous step, which determines the direction of the step, and the frequency f_{Si+1} of the excitation source (the AWG in this case) is changed, accordingly. The number of steps in this work is set to $M = 11$.

To enhance the computational efficiency and improve frequency resolution, the algorithm employs variable frequency steps. The search algorithm initiates by evaluating the response amplitude at the boundary frequencies, $f_{\Delta\,\max}$ and $f_{\Delta\,\min}$, of the chosen interval ($\Delta f = f_{\Delta\,\max} - f_{\Delta\,\min}$). It then proceeds to search for the peak using a coarse approach with $M' = 5$ steps, each 100 Hz wide (including the two starting points at $f_{\Delta\,\max}$ and $f_{\Delta\,\min}$). This coarse span covers frequencies that are far from the potential peak frequency. Subsequently, the algorithm continues processing the remaining M–M' steps by halving the step width at each iteration with a dichotomic scheme.

By employing variable width steps and combining coarse and refined search strategies, the algorithm aims to reduce computing time while achieving a higher accuracy in locating the resonance peak.

In this work, the frequency searching interval is $\Delta f = 500$ Hz; it follows that the last step has a width of 1.56 Hz that corresponds to the resolution of the search and tracking algorithm and is proven to also determine its accuracy.

IV. Experimental Results and Discussion

The feasibility of the proposed dual gas sensing method has been investigated by experimental tests in the reference conditions described in Section III-B. During measurements, the performance of the frequency tracking algorithm and of the evaluation of the PA signal was characterized by exposing the system to different concentrations of CO_2 in the range between 0% and 8%, and of NO_2 in the range between 0 and 50 ppm, in pure N_2 as carrier gas. The measurement system is set to perform one peak measurement in about 2 s

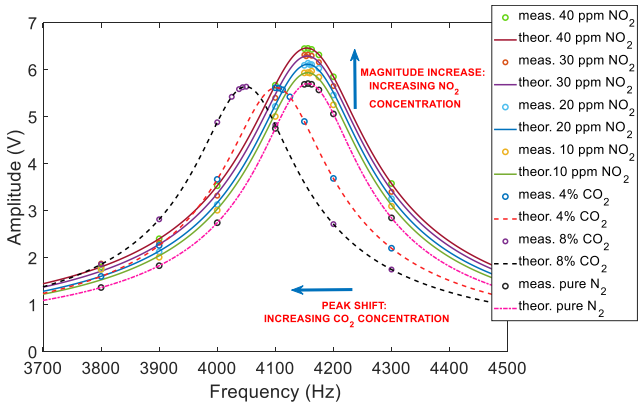

Fig. 7. Output of the RFT algorithm, f_{si} $i = 1, \ldots, 11$ (markers) in different measurement conditions (different CO_2 and NO_2 concentrations) as per legend, represented in the frequency domain. The solid and dashed lines represent the fittings of the theoretical frequency response of the resonator.

during which the designed search and tracking algorithm is executed. As described in Section III-C, the algorithm takes $M = 11$ steps, each one about 200 ms long, to track the resonance frequency of the resonator. The results obtained during the RFT algorithm are presented in Fig. 7. The figure, which serves as an illustrative tool to elucidate the sensing mechanisms, presents different situations obtained in different gas mixtures as described in the legend. The measurements performed during the RFT algorithm execution are displayed in terms of frequency and PA signal amplitude as markers, illustrating all the intermediate results obtained during the execution of the M steps (11 points). These M points actually sample the PA cell resonant response in the different tested conditions. Fig. 6 also includes lines representing the results of curve fittings, where the measurement data fits with the theoretical responses of the resonator (i.e., $|P(f)| = (G_r/((1 - ((f/f_r))^2)^2 + ((f/Q_r f_r))^2)^{1/2}))$, where G_r is the dc gain of the system) showing the adherence of the resonant behavior of the PA cell to the expected one (a resonant system with a Q-factor of 28). It can be seen how the spectral response of the system is affected by the presence of the two target gases in accordance with the behavior described in Sections II and III, i.e., the light is not absorbed by the CO_2 gas; hence, its presence in large concentrations only affects the sound speed and shifts the resonance frequency of the chamber but not the PA signal magnitude. On the other hand, NO_2 absorbs the optical power, and the amplitude of the PA signal increases with its concentration, whereas, since its concentration is in the ppm range, the influence on the sound speed and the consequent frequency shift can be neglected.

Even in the absence of NO_2, i.e., in the absence of any gas with an absorption peak tuned to the used optical wavelength, there is a large PA signal, which, moreover, represents the background (pure N_2 test case). This can be due to nonspecific adsorption of the gas species and of the solid parts of the chamber, sometimes called "wall noise," [23] whereas the presence of 40 ppm of NO_2 increases the PA signal amplitude by about 20%.

Fig. 8(a) shows the results of the RFT algorithm obtained by varying the concentration of CO_2, using N_2 as the carrier gas

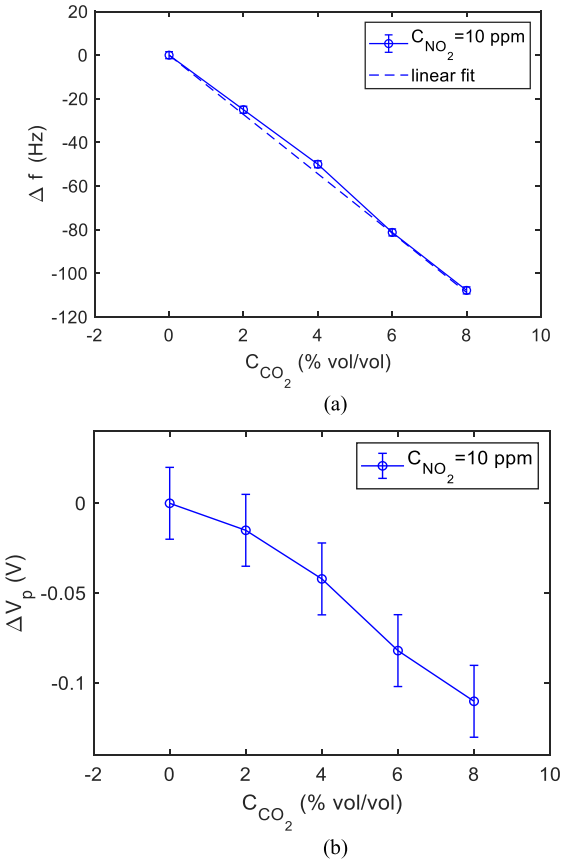

Fig. 8. (a) Measured frequency shift and (b) PA signal amplitude at the tracked resonance frequency as a function of the CO_2 concentration, with N_2 as the carrier gas and fixed concentration of NO_2 set as 10 ppm vol/vol; total flow 100 mLl/min.

and with a fixed concentration of NO_2. It can be seen that in the tested range, the relationship between CO_2 concentration and measured resonance frequency shift Δf is quite linear, with NLE lower than 0.3% of the spanned range and with a slope of the linear fit equal to 11.9 Hz/%CO_2, which corresponds to a satisfactory sensitivity. In fact, considering that the search algorithm has a resolution of about 1.6 Hz, this means a resolution of CO_2 concentration of about 0.2%CO_2 in the target application (0.13%CO_2 in the laboratory tests). These results are perfectly explainable with the expected variations of the sound speed due to the presence of CO_2. In fact, as shown in Fig. 4, the presence of 8% of CO_2 causes a relative variation of the sound speed of 2.5%; correspondingly, the measured resonant frequency shift is 100 Hz, corresponding to 2.5% of the resonance frequency in the absence of CO_2.

In Fig. 8(b), the estimated amplitude of the PA signal is shown, and it can be seen that its variations, ΔV_p, in the tested range, are little, and smaller than a few tens of millivolts. This is important because any variation of the PA signal amplitude due to the CO_2 presence causes an error in the NO_2 measurement that relies on amplitude detection.

The system response to variable NO_2 concentration, with a fixed concentration of CO_2 and N_2 as the carrier gas, is reported in Fig. 9(a), which shows the output of the RFT algorithm in terms of estimated resonance frequency in the presence of different concentrations of NO_2, from 0 to 50 ppm,

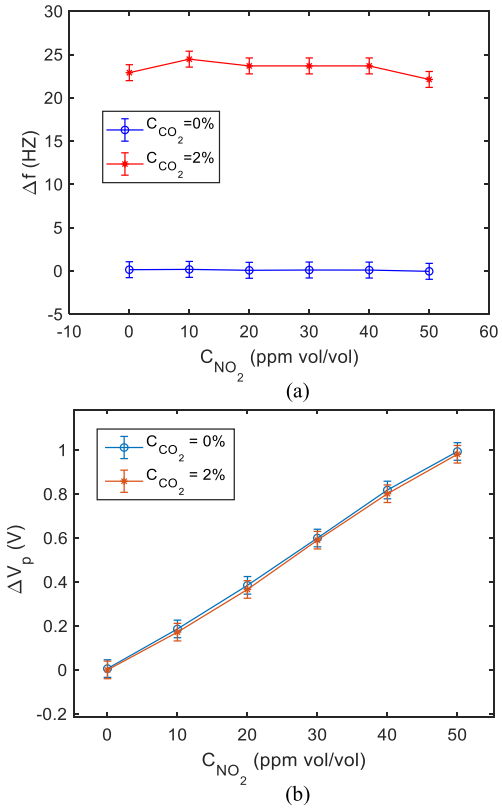

Fig. 9. (a) Measured frequency shift and (b) PA signal amplitude at the tracked resonance frequency as a function of the NO_2 concentration, with nitrogen as the carrier gas and fixed concentration of CO_2 set as 2% vol/vol; total flow 100 mL/min.

TABLE II
MEASUREMENT RESULTS IN DIFFERENT TEST CONDITIONS

test condition	ΔV_p (V)	Δf (Hz)
C_{CO2}=0%		
C_{NO2}=10 ppm ±1.2 ppm	0.19 ±0.013	1.2. ±0.92
C_{NO2}=20 ppm ±2.3 ppm	0.38 ±0.013	-1.0 ±0.92
C_{NO2}=30 ppm ±3.4 ppm	0.59 ±0.013	-0.9 ±0.92
C_{CO2}=4% ±0.1%		
C_{NO2}=10 ppm ±1.2 ppm	0.18 ±0.013	-47.1 ±0.92
C_{NO2}=20 ppm ±2.3 ppm	0.37 ±0.013	-46.4 ±0.92
C_{NO2}=30 ppm ±3.4ppm	0.58 ±0.013	-47.7 ±0.92
C_{CO2}=8% ±0.15%		
C_{NO2}=10 ppm ±1.2 ppm	0.19 ±0.013	-94.3 ±0.92
C_{NO2}=20 ppm ±2.3 ppm	0.39 ±0.013	-93.5 ±0.92
C_{NO2}=30 ppm ±3.4 ppm	0.57 ±0.013	-95.1 ±0.92

whereas Fig. 9(b), shows the results obtained by the searching algorithm in terms of PA signal amplitude, as a function of NO_2 concentration. It can be seen that the amplitude response is pretty linear with a sensitivity of about 20 mV/ppm NO_2; correspondingly, the errors due to the maximum possible variation of CO_2 concentration in the application of interest (2.5%CO_2 in test conditions) are equivalent to uncertainty on NO_2 concentration measurement smaller than 1 ppm.

Finally, the proposed technique performance is summarized in Table II, where measurement results are reported together with the estimated combined standard uncertainty.

V. CONCLUSION

In this article, an effective technique for the simultaneous measurement of the concentration of NO_2 and CO_2 in the exhaust gases of industrial plants is presented. The proposed methodology can be extended to any gas analyzer devoted to the measurements of compounds with very different concentration ranges by appropriately selecting the optical source or sources for the detection of gases with concentration in the ppm range while exploiting the sound speed variation for the detection of gases with concentrations in higher ranges. We performed experimental validations to assess the feasibility of simultaneously detecting the two target gas species; experimental results show the possibility to detect NO_2 with a resolution lower than 1 ppm, whereas CO_2 resolution is about 0.2%. The technique exploits PA detection boosted by acoustic resonant measurement cells. The proposed system allows the detection of two gases by a unique sensor, which is simple and robust, both as far as the optical components required (simply an LED), the mechanical structure of the cell, which, as discussed in [31] allows for an easy mounting and positioning of the optical source, microphone, and gas inlet and outlet. Regarding the hardware configuration, the measurement setup represents a scalable solution as it can be readily adjusted for the detection of various gases, even those found in low concentration within the examined flow, by simply choosing a different light source. Finally, as far as the electronics is concerned, the system is based mainly on ad hoc designed front-end circuits and on instruments. Indeed, in accordance with the operational specification of the system, the AWG, the acquisition board, and the PC used for the validation of the proposed sensing system can be easily replaced by suitable low-cost embeddable electronic components such as a Direct Digital Synthesizer (DDS) and a microcontroller; therefore, the developed system is not only useful to give a proof of concept for the proposed measurement technique, but it can be seen as the prototype for a stand-alone low-cost sensor.

Summarizing, the novelty of the proposed approach lies in its uses of RFT, a crucial element for achieving the necessary precision in detecting target gas (NO_2) with resolution within a part per million (ppm), in environments where variations in sound speed occur due to different working conditions, including fluctuations in carrier gas composition. We have demonstrated the feasibility of using RFT as a direct measurement of CO_2 concentration in the discussed application. Furthermore, the exploitation of a ring-shaped resonator as the PA cell structure not only ensures a high sensitivity but also facilitates the incorporation of straightforward, cost-effective conditioning electronics. As a result, our method represents both a breakthrough and a practical advancement in the field of exhaust gas monitoring.

REFERENCES

[1] H. Hanachi, C. Mechefske, J. Liu, A. Banerjee, and Y. Chen, "Performance-based gas turbine health monitoring, diagnostics, and prognostics: A survey," *IEEE Trans. Rel.*, vol. 67, no. 3, pp. 1340–1363, Sep. 2018, doi: 10.1109/TR.2018.2822702.

[2] M. Tahan, E. Tsoutsanis, M. Muhammad, and Z. A. Abdul Karim, "Performance-based health monitoring, diagnostics and prognostics for condition-based maintenance of gas turbines: A review," *Appl. Energy*, vol. 198, pp. 122–144, Jul. 2017.

[3] *Ambient Air Quality Database, 2022 Update: Status Report*, World Health Organization, Geneva, Switzerland, 2022.

[4] A. Fentaye, A. Baheta, S. Gilani, and K. Kyprianidis, "A review on gas turbine gas-path diagnostics: State-of-the-art methods, challenges and opportunities," *Aerospace*, vol. 6, no. 7, p. 83, Jul. 2019, doi: 10.3390/aerospace6070083.

[5] W. Zeng, L. Pang, W. Zheng, and E. Hu, "Study on combustion and emission characteristics of a heavy-duty gas turbine combustor fueled with natural gas," *Fuel*, vol. 275, Sep. 2020, Art. no. 117988.

[6] T. Addabbo, A. Fort, M. Mugnaini, E. Panzardi, and V. Vignoli, "Measurement system based on electrostatic sensors to detect moving charged debris with planar-isotropic accuracy," *IEEE Trans. Instrum. Meas.*, vol. 68, no. 3, pp. 837–844, Mar. 2019.

[7] P. Roointon and G. D. Moore, "Gas turbine emissions and control," *Atlanta, GE Energy Services*, vol. 1, pp. 1–20, Mar. 2001. [Online]. Available: https://www.eplptx.com/wp-content/uploads/2020/05/Gas-Turbine-Emissions-and-Control.pdf

[8] M. Masiol and R. M. Harrison, "Aircraft engine exhaust emissions and other airport-related contributions to ambient air pollution: A review," *Atmos. Environ.*, vol. 95, pp. 409–455, Oct. 2014.

[9] S. McAllister, J. Y. Chen, and A. C. Fernandez-Pello, *Fundamentals of Combustion Processes* (Mechanical Engineering Series). New York, NY, USA: Springer, 2011.

[10] Environmental Protection Agency. *National Emission Standards for Hazardous Air Pollutants Stationary Combustion Turbines Amendments*. Federal Register. Accessed: Jul. 17, 2023. [Online]. Available: https://www.federalregister.gov/documents/2022/03/09/2022-04848/national-emission-standards-for-hazardous-air-pollutants-stationary-combustion-turbines-amendments

[11] P. Q. Tranchida, "Gas chromatography multidimensional," in *Encyclopedia of Analytical Science*, P. L Worsfold, C. Poole, A. Townshend, and M. L. Miro, Eds., 3rd ed. Cambridge, MA, USA: Academic Press, 2019, pp. 202–216.

[12] B. P. Regmi and M. Agah, "Micro gas chromatography: An overview of critical components and their integration," *Anal. Chem.*, vol. 90, no. 22, pp. 13133–13150, Nov. 2018.

[13] M. Chowdhury et al., "Miniaturized gas chromatographic nose for on-site adulteration detection," *IEEE Trans. Instrum. Meas.*, vol. 72, pp. 1–11, 2023.

[14] R. K. Jha, "Non-dispersive infrared gas sensing technology: A review," *IEEE Sensors J.*, vol. 22, no. 1, pp. 6–15, Jan. 2022, doi: 10.1109/JSEN.2021.3130034.

[15] M. Hilton, A. H. Lettington, and C. W. Wilson, "Gas turbine exhaust emissions monitoring using nonintrusive infrared spectroscopy," *J. Eng. Gas Turbines Power*, vol. 120, no. 3, pp. 514–518, Jul. 1998.

[16] Z. Xi et al., "Near-infrared dual-gas sensor system for methane and ethane detection using a compact multipass cell," *Frontiers Phys.*, vol. 10, p. 107, Mar. 2022.

[17] Y. Wang, M. Nakayama, M. Yagi, M. Nishikawa, M. Fukunaga, and K. Watanabe, "The NDIR CO_2 monitor with smart interface for global networking," *IEEE Trans. Instrum. Meas.*, vol. 54, no. 4, pp. 1634–1639, Aug. 2015, doi: 10.1109/TIM.2005.851474.

[18] S. Palzer, "Photoacoustic-based gas sensing: A review," *Sensors*, vol. 20, no. 9, p. 2745, May 2020.

[19] F. Wang et al., "Techniques to enhance the photoacoustic signal for trace gas sensing: A review," *Sens. Actuators A, Phys.*, vol. 345, Oct. 2022, Art. no. 113807.

[20] A. Miklós, P. Hess, and Z. Bozóki, "Application of acoustic resonators in photoacoustic trace gas analysis and metrology," *Rev. Sci. Instrum.*, vol. 72, no. 4, pp. 1937–1955, Apr. 2001.

[21] A. Fort, E. Panzardi, V. Vignoli, E. Landi, M. Mugnaini, and K. S. Drese, "NO_2 photoacoustic sensing system based on resonant cell and UV-LED sensor," in *Proc. IEEE Int. Workshop Metrology Ind. 4.0 IoT*, Jun. 2021, pp. 583–587.

[22] L. D. Landau and E. M. Lifshitz, *Statistical Physics*, vol. 5. Amsterdam, The Netherlands: Elsevier, 2013.

[23] C. Weber, J. Kapp, J. Wöllenstein, and K. Schmitt, "Novel approach for efficient resonance tracking in photoacoustic gas sensor systems based on a light-induced wall signal," *Photoacoustics*, vol. 31, Jun. 2023, Art. no. 100495.

[24] A. J. Zuckerwar, *Handbook of the Speed of Sound in Real Gases*. Cambridge, MA, USA: Academic Press, 2002.

[25] K. Liu, L. Dong, and F. K. Tittel, "Compact sound-speed sensor for quartz enhanced photoacoustic spectroscopy based applications," *Rev. Sci. Instrum.*, vol. 86, no. 4, Apr. 2015, Art. no. 044903, doi: 10.1063/1.4918796.

[26] T. Löfqvist, J. Delsing, and K. Sokas, "Speed of sound measurements in gas-mixtures at varying composition using an ultrasonic gas flow meter with silicon based transducers," in *Proc. Int. Conf. Flow Meas.*, May 2003, pp. 12–14.

[27] J. Wang, M. Chen, Q. Chen, Y. An, Z. Feng, and H. Wang, "Photoacoustic spectrometry and resonant frequency tracking based dual-mode gas sensor," *Sens. Actuators B, Chem.*, vol. 390, Sep. 2023, Art. no. 133796.

[28] A. G. Bell, "Upon the production of sound by radiant energy," *Lond., Edinb., Dublin Philos. Mag. J. Sci.*, vol. 11, no. 1881, pp. 510–528, 2023.

[29] A. Rosencwaig and A. Gersho, "Theory of the photoacoustic effect with solids," *J. Appl. Phys.*, vol. 47, no. 1, pp. 64–69, Jan. 1976, doi: 10.1063/1.322296.

[30] T. Rück, R. Bierl, and F.-M. Matysik, "Low-cost photoacoustic NO_2 trace gas monitoring at the pptV-level," *Sens. Actuators A, Phys.*, vol. 263, pp. 501–509, Aug. 2017.

[31] A. Fort, M. Mugnaini, E. Panzardi, V. Vignoli, F. Dötzer, and K. S. Drese, "Highly sensitive photoacoustic NO_2 measurement system based on an optimized ring-shaped resonant cell," *IEEE Trans. Instrum. Meas.*, vol. 72, pp. 1–10, 2023.

[32] D. C. Dumitras, D. Dutu, C. Matei, A. M. Magureanu, M. Petrus, and C. Popa, "Laser photoacoustic spectroscopy: Principles, instrumentation, and characterization," *J. Optoelectron. Adv. Mater.*, vol. 9, pp. 3655–3701, Dec. 2007.

[33] A. O. Markano and V. T. Platonenko, "Saturation of light absorption in molecular gases," *Sov. J. Quantum Electron.*, vol. 9, no. 5, pp. 563–565, May 1979.

[34] M. Suchenek and T. Borowski, "Measuring sound speed in gas mixtures using a photoacoustic generator," *Int. J. Thermophys.*, vol. 39, no. 1, p. 11, Jan. 2018.

[35] (2023). *HITRAN Database*. [Online]. Available: https://hitran.org

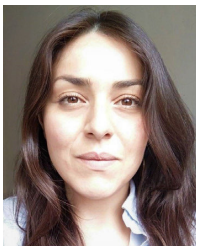

Enza Panzardi (Member, IEEE) received the master's degree in electronics and communication engineering and the Ph.D. degree in information engineering and science from the University of Siena, Siena, Italy, in 2015 and 2019, respectively.

She is currently a Research Associate with the Electronics and Electronics Measurement Research Group, University of Siena. Her current research interests include electronic circuits and systems for industrial applications and chemical-sensor-based measurement systems.

Klaus Stefan Drese received the master's degree in physics from the State University of New York, Buffalo, NY, USA, in 1993, the Diploma degree in physics from University of Würzburg, Würzburg, Germany, in 1995, and the Ph.D. degree from the University of Marburg, Marburg, Germany, in 1998.

He was a Scientific Director with the Fraunhofer Institute for Microengineering and Microsystems (formerly IMM GmbH), Mainz, Germany, until 2016. He is currently a Professor of sensor and actuator technology and microacoustic with the Coburg University of Applied Sciences and Arts, Coburg, Germany, and the Head of the Institute of Sensor and Actuator Technology (ISAT), Coburg. He does research in computational physics, microfluidics, and theoretical and acoustic physics.

Marco Mugnaini received the Laurea degree in electronic engineering and the Ph.D. degree in reliability, availability, and logistics from the University of Florence, Florence, Italy, in 1999 and 2003, respectively.

Since 2003, he has been a Product Safety Engineer with General Electric Oil and Gas Business, Florence. Since 2005, he has been an Assistant Professor with the Department of Information Engineering, University of Siena, Siena, Italy. His current interests include the development of measurement systems based on chemical sensors.

Dr. Mugnaini received the Green Belt Certification from General Electric Oil and Gas.

Lorenzo Parri received the M.Sc. degree in electronics and communications engineering and the Ph.D. degree in information engineering and science from the University of Siena, Siena, Italy, in 2017 and 2021, respectively.

He is currently a Research Fellow with the Department of Information Engineering and Mathematics, University of Siena. His current research interests include the design of gas measurement systems, electronic systems for industrial application and condition monitoring, the design of embedded microcontroller-based devices, and the development of sensor networks.

Valerio Vignoli (Member, IEEE) received the Laurea degree in electronic engineering and the Ph.D. degree in nondestructive testing from the University of Florence, Florence, Italy, in 1989 and 1994, respectively.

He is currently a Full Professor of electronics with the Department of Information Engineering and Mathematical Sciences, University of Siena, Siena, Italy. His current research interests include the design of data acquisition and processing systems based on chemical sensors and the design of analog and mixed-signal electronic circuits.

Ada Fort (Member, IEEE) received the Laurea degree in electronic engineering and the Ph.D. degree in nondestructive testing from the University of Florence, Florence, Italy, in 1989 and 1992, respectively.

She is currently a Full Professor with the Department of Information Engineering and Mathematical Sciences, University of Siena, Siena, Italy. Her current research interests include the development of measurement systems based on chemical and ultrasonic sensors and the development of automatic fault diagnosis systems. Recently, she has been involved in the study of random number generators based on chaotic maps.

Open Access funding provided by 'Università degli Studi di Siena' within the CRUI CARE Agreement